Journal of
MATERIALS RESEARCH

Determination of indenter tip geometry and indentation contact area for depth-sensing indentation experiments

K. W. McElhaney, J. J. Vlassak, and W. D. Nix
Department of Materials Science and Engineering, Stanford University, Stanford, California 94305

(Received 26 September 1996; accepted 31 October 1997)

The phenomena of pile-up and sink-in associated with nanoindentation have been found to have large effects on the measurements of the indentation modulus and hardness of copper. Pile-up (or sink-in) leads to contact areas that are greater than (or less than) the cross-sectional area of the indenter at a given depth. These effects lead to errors in the absolute measurement of mechanical properties by nanoindentation. To account for these effects, a new method of indenter tip shape calibration has been developed; it is based on measurements of contact compliance as well as direct SEM observations and measurements of the areas of large indentations. Application of this calibration technique to strain-hardened (pile-up) and annealed (sink-in) copper leads to a unique tip shape calibration for the diamond indenter itself, as well as to a material parameter, α, which characterizes the extent of pile-up or sink-in. Thus the shape of the indenter tip and nature of the material response are separated in this calibration method. Using this approach, it is possible to make accurate absolute measurements of hardness and indentation modulus by nanoindentation.

I. INTRODUCTION

Indentation experiments have led to well-established methods for determining the mechanical properties of materials in small volumes.[1–9] The availability of depth-sensing indentation instruments with capabilities for measuring displacements on the order of nanometers now makes it possible to study mechanical properties of thin films and other finely structured materials where small volumes need to be probed.[1,4] Research on nanoindentation has shown that elastic moduli,[2,4,7,10] hardness,[1,35] and time-dependent deformation effects[11] can be measured, provided the area of contact between the indenter and the test material is known. Indeed, determining the contact area from the indentation forces and displacements is central to the study of mechanical properties of materials in small volumes by nanoindentation.

It is widely known that the contact area at a particular depth of indentation depends not only on the shape of the indenter (diamond) but also on the elastic-plastic response of the material being indented. In some cases the volume of material displaced by the indentation pushes out to the sides of the indenter and forms a pile-up of material, making the projected contact area larger than the cross-sectional area of the indenter at that depth. For other materials, the displaced volume is accommodated mainly by far-field elastic displacements, producing what is called a sink-in effect. In this case the contact area is less than the cross-sectional area of the indenter at that depth.

Although the pile-up and sink-in effects are widely known, they are not explicitly considered in any of the current methods for determining contact areas from indentation loads and displacements. Typically the variations of contact area with depth are treated as indicating the shape of the diamond indenter itself.[6,7] This approach to calibrating the shape of the indenter is not generally valid as it mixes the actual shape of the diamond indenter with the elastic-plastic response of the material used for the tip shape calibration. Naturally such a "combined" tip shape calibration will return accurate contact areas only if the material being subsequently studied exhibits the same pile-up or sink-in behavior as the material used for the calibration experiments.

In this paper we develop a new technique for determining the indenter tip shape using both indentation loads and displacements and direct scanning electron microscopy (SEM) images of the impressions left by large indentations. The indenter tip shape found by this method represents the actual cross-sectional area of the indenter as a function of the distance from the tip. This new tip shape calibration can then be used in nanoindentation studies of other materials, regardless of their pile-up or sink-in behaviors. For the determination of contact area, the extent of pile-up or sink-in must be measured for each material by making direct observations of the impressions made by large indentations. In this way we separate the indenter tip shape calibration (which needs to be done only once) from the pile-up or sink-in response of the material (which must be done each time a new material is studied).

A. Background

Here we describe some of the basic quantities and analytical relations that are used in nanoindentation to determine contact areas from the measured loads and dis-

placements. Because the displacements during unloading are elastic, the relationship between the unloading curve and the elastic modulus of the material being tested can be described by elastic contact theory. Pharr, Oliver, and Brotzen[8] have shown that the compliance of the contact between any axisymmetric indenter and an elastically isotropic half-space is given by

$$C_c = \frac{dh}{dP} = \frac{\sqrt{\pi}}{2}\frac{1}{\sqrt{A}}\frac{1}{E_r}, \quad (1)$$

where E_r is a reduced modulus described by the relationship

$$\frac{1}{E_r} = \left(\frac{1-\nu^2}{E}\right)_{\text{specimen}} + \left(\frac{1-\nu^2}{E}\right)_{\text{indenter}}, \quad (2)$$

and where E and ν are Young's modulus and Poisson's ratio, respectively. Here h is the displacement of the indenter relative to the specimen, P is the load, and A is the projected area of contact between the specimen and the indenter. Equations (1) and (2) can also be generalized for elastically anisotropic materials; if the indentation modulus is properly defined, the basic form of these equations does not change.[10,12] To account for elastic displacements of the load frame of the instrument, the machine compliance, C_m, must be added to the contact compliance, C_c, to obtain the overall or total compliance of the testing system,

$$C_{\text{total}} = C_m + C_c = C_m + \frac{\sqrt{\pi}}{2}\frac{1}{E_r}\frac{1}{\sqrt{A}}. \quad (3)$$

The linear relationship between C_{total} and $A^{-1/2}$ for indentations of several depths is used to determine the machine compliance, which is simply the intercept of this curve. The contact compliance is then the difference between the measured total compliance and the experimentally determined machine compliance. Once the contact compliance is known, the indentation modulus of the specimen can be calculated.

In the usual way we define the hardness of the material to be the mean pressure exerted by the indenter at maximum load,

$$H = \frac{P_{\max}}{A}, \quad (4)$$

where $P_{\max}$ is the maximum load applied during the indentation and A is, again, the projected area of contact between the indenter and the specimen.

The measurements of indentation modulus and hardness depend on knowing the contact area of the indentations. The contact area is determined from a tip shape function, $A(h_c)$, that expresses the indenter's cross-sectional area in terms of the contact depth and must be determined for each indenter tip used in an experiment. The contact depth (or plastic displacement) is determined by expressing the total measured displacement ($h_{\max}$) as the sum of the elastic surface displacement (h_s) and the contact depth. It then follows that $h_c = h_{\max} - h_s$. Two models that have been widely used to determine contact depth are those of Doerner and Nix,[4] who model the indenter as a flat punch and assume initial unloading to be linear, and Oliver and Pharr,[7] who treat the indenter as a paraboloid of revolution and describe the unloading curve by a power law.

B. Indenter-tip calibration

To make accurate measurements by indentation experiments, the contact areas of the indentations must be precisely known. As noted above, it is standard practice to assume that the area of contact for an indentation of a specified depth is the cross-sectional area of the diamond indenter tip at that depth. In this practice the geometry of the tip is described by an area function $A(h_c)$ and this function is used to determine the contact area of an indentation made to a prescribed depth.

One method for determining the area function of a tip involves imaging the indentations. The calibration is made by fitting the imaged areas at known depths to an area function. However, optical imaging of submicron indentations is difficult, and SEM imaging does not provide sufficient contrast to discern the area of contact for shallow indentation. Doerner and Nix[4] described an indenter-tip calibration using transmission electron microscopy (TEM) images of indentation replicas, but this method is somewhat inconvenient, being both expensive and time-consuming.

Currently, the most popular method for calibrating the shape of the indenter tip is the one introduced by Oliver and Pharr.[7] It is based on the measurement of contact stiffness and requires no imaging of the indentations. The method involves first making large indentations in a soft material such as aluminum and assuming that the tip exhibits ideal Berkovich geometry, described by the area function

$$A(h_c) = 24.5h_c^2, \quad (5)$$

where h_c is the indentation contact depth determined by the method of Oliver and Pharr.[7] Then from the plot of C_{total} versus $A^{-1/2}$, an initial estimate of the machine compliance can be determined from the two largest indentations, using literature values of E and ν for aluminum and diamond. Contact areas for all the depths are then calculated from Eq. (3), and the data are fitted to a polynomial function $A(h_c)$. Since the new area function yields a new value of C_m, the process is iterated until convergence is achieved. To determine the tip geometry at shallower depths, a similar method involving indentations in fused quartz is used, assuming the same machine compliance as measured

in the aluminum experiments. This area function is assumed to describe the tip geometry completely, and thus it yields the contact area of any indentation made to a known depth. In this approach the cross-sectional area of the tip and the contact area of the indenter and the specimen, at a given depth, are treated implicitly as if they are the same.

C. Pile-up and sink-in

The strain-hardening properties of a material can affect its behavior underneath the indenter tip. (See Fig. 1 for a schematic representation of these effects). A well-annealed soft metal that exhibits a high strain-hardening rate will tend to show far-field plasticity. Strain hardening near the indenter tip will cause plastic deformation to occur further and further away from the contact, causing material to be displaced far away from the indentation and resulting in sink-in behavior. This sinking-in of the surface causes the actual contact area to be less than the cross-sectional area of the indenter at that depth. By contrast, strain-hardened materials and metallic glasses that exhibit a low strain-hardening rate will deform more locally, creating a pile-up of material against the sides of the indenter. This displacement of material near the indentation results in a significant increase in contact area at a given depth.

Figure 2 shows SEM images of two indentations made to the same depth in different samples of copper. The pile-up and sink-in behaviors are evident in the images. That the areas of indentations made to the same depth with the same indenter can be so different indicates that a distinction must be made between the area of the diamond indenter and the actual contact area of the indentation. Although an area function may be obtained that describes the geometry of the indenter, for materials that show large pile-up or sink-in effects, a distinction must be made between the contact area and the cross-sectional area of the indenter. Such a distinction is necessary to obtain accurate measurements of contact areas and, correspondingly, accurate determinations of hardnesses and indentation moduli.

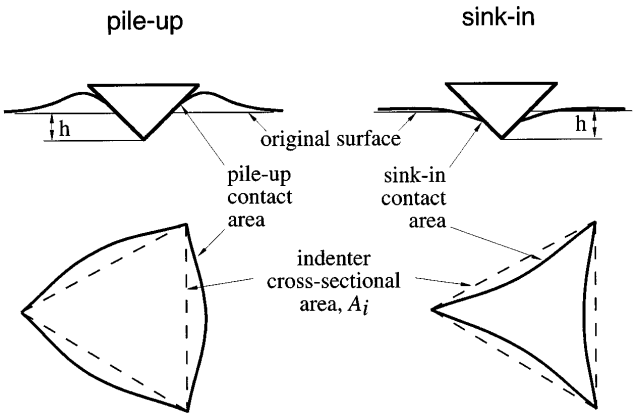

FIG. 1. A schematic representation of pile-up and sink-in effects during indentation.

II. EXPERIMENTAL

A. Description of indentation experiments

Indentation experiments were conducted using a Nanoindenter®, a low-load, displacement-sensing indentation system manufactured by Nano Instruments. Experiments were done using two samples of copper, one that was strain-hardened and one that had been annealed. The strain-hardened sample was polycrystalline with a grain size that was large compared to the size of the large indentations, so of the indentations were made in single grains. The annealed sample was a single crystal of copper with the (111) orientation. The samples were prepared by successive grinding steps with sandpaper down to 600 grit, and polishing steps with 1 μm diamond paste on nylon cloth and 0.06 μm colloidal silica on RAYVEL®.

Experiments consisted of arrays of thirty-six indentations, each array spanning six different depths. Two arrays were made for each of four depth ranges, which spanned the entire testing range of 20 nm to 2 μm. The data from each of the twelve indentations made to the same depth were averaged. A typical loading sequence and the corresponding load-displacement curve for the experiments is shown in Fig. 3. A curve fit in the form of a power law was made to the upper 60% of the final unloading data, and contact compliance and contact depth were calculated from this fit using the method of Oliver and Pharr.[7] Experiments in a single sample were done without changing the sample mounting and on the same area of the sample to ensure that the machine compliance would remain constant from experiment to experiment.

B. Determination of machine compliance and reduced modulus

To determine the machine compliance, the largest six indentation depths were imaged by SEM, and their areas were determined by tracing all twelve indentations at those depths onto transparency film and weighing the cut-outs. Precise magnification of the SEM images was determined by measuring the distances between indentations on the sample with the Nanoindenter and then comparing them with the distances on the micrographs. The total measured compliance was plotted versus the reciprocal square root of the measured contact areas; the machine compliance, C_m, was determined from the intercept of this plot, and the reduced modulus, E_r, from the slope. Figure 4 is a compliance versus contact area plot showing the machine compliance in these experiments to be about 2.1 nm/mN. The moduli

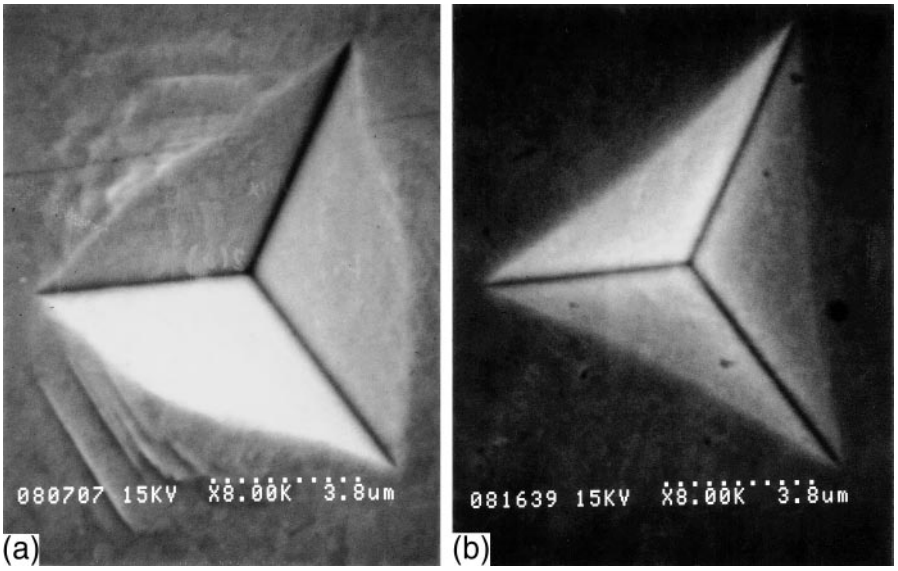

FIG. 2. SEM micrographs of 1500 nm deep indentations in (a) strain-hardened copper (pile-up) and (b) annealed copper (sink-in).

determined for these copper samples agree with those calculated by Vlassak and Nix[10] (see Table I).

C. Determination of tip area function

To distinguish between the contact area of the indentation and the cross-sectional area of the indenter at that depth, we again used the SEM images, but took the indenter area to be that of the triangle defined by the indentation corners. In doing this, two assumptions are made: (i) that the sides of the diamond indenter are flat, so the cross section of the diamond at any depth is indeed represented by a triangle, and (ii) that little pile-up or sink-in occurs at the sharp edges of the indenter, so that most of the material displacement occurs against the flat sides of the diamond. The second assumption is verified by the observation that the "triangular areas" of indentations made to the same depth in the two materials were almost exactly equal.

A parameter describing the ratio of the indentation contact area to the triangular area was then determined for each set of indentations:

$$\alpha = \frac{A_c}{A_i} . \tag{6}$$

Here A_c refers to the indentation projected contact area, and A_i to the cross-sectional area of the indenter, the area of the triangle marked by the corners of the indentation. For an indentation where pile-up has occurred, $\alpha > 1$; for sink-in, $\alpha < 1$. Rearranging Eq. (1) and substituting Eq. (6), the diamond tip area can then be determined from the measured contact compliances using

$$A_i = \frac{1}{\alpha} \frac{\pi}{4} \frac{1}{E_r^2} \frac{1}{C_c^2} . \tag{7}$$

Thus, the cross-sectional area of the indenter can be calculated using the measured contact compliances at all the indentation depths, provided the correction factor α is known at each depth. If indenter geometry is self-similar at all depths, α should be independent of depth for a homogeneous material.

III. RESULTS AND DISCUSSION

The calibration procedure outlined above was performed on each of the two copper samples. Figure 5 shows a logarithmic plot of the final area function as determined by experiments in each sample. Their agreement further corroborates the validity of the assumption that the sharpness of the edges of the indenter produces little pile-up or sink-in behavior at the corners of the indentation.

The tip calibration method of Oliver and Pharr is based entirely on the measurement of contact compliance; it does not make use of or require direct observations of any of the indentations. Provided that the material used for the calibration shows neither pile-up nor sink-in effects, an accurate tip shape calibration can be found. However, such a tip shape calibration cannot be used without modification for the study of other materials if they show either pile-up or sink-in effects. Significant errors in the contact area will produce correspondingly large errors in the measurement of indentation modulus and hardness. Also, Baker and Nix[13] have reported that the machine compliance can vary significantly from sample to sample, and can even depend on the location of indentations in a single sample. If the machine compliance is not accurately known, convergence of the iterative process may be difficult to achieve. For this reason to it is preferable to com-

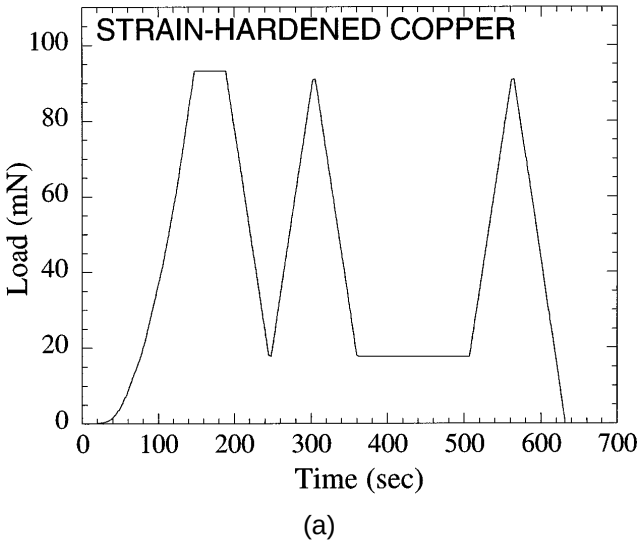

(a)

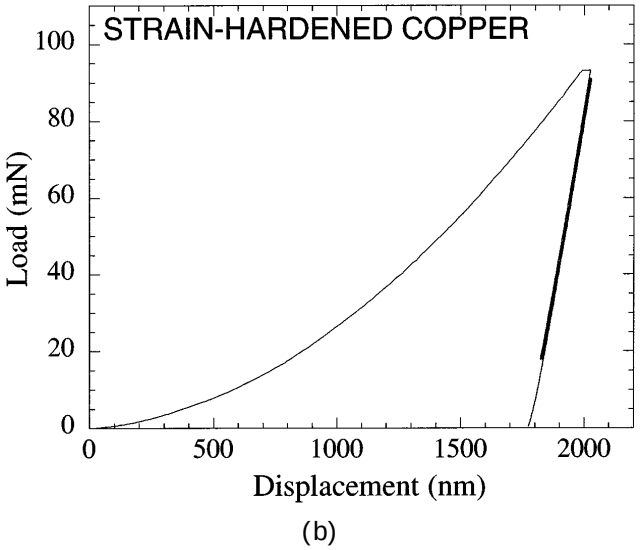

(b)

FIG. 3. (a) A typical indentation load-time sequence. (b) Corresponding load-displacement curve for an indentation in strain-hardened copper.

bine the measurement of contact compliance with direct observations of the indentations.

Figure 6 shows a plot of α as a function of depth for the strain-hardened and the annealed copper samples. Note that for the strain-hardened specimen, the value of α is constant over the entire range of depths, indicating that the amount of strain-hardening in the sample is independent of depth. This sample is a suitable material in which to perform a tip calibration, for it is homogeneously strain-hardened, and its pile-up behavior remains constant throughout. For the annealed crystal, however, α increases significantly with decreasing depth. The most probable cause of this behavior is that the surface of the annealed crystal was strain-hardened during the metallographic preparation. Thus, shallow indentations are more likely to pile-up than

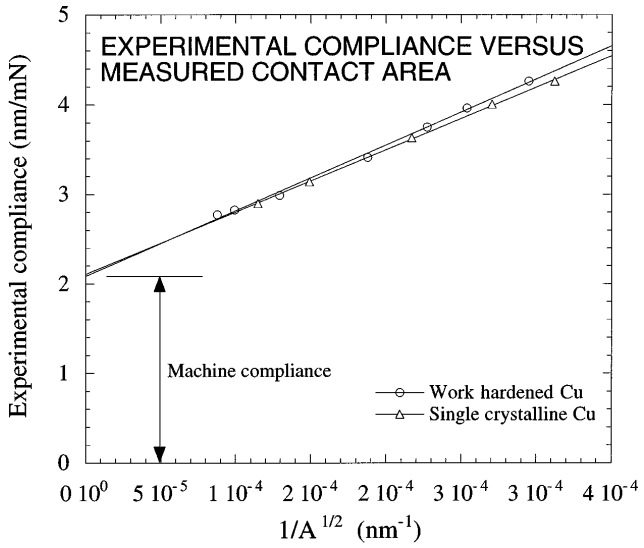

FIG. 4. Measured compliance versus contact area for both annealed and strain-hardened copper showing a machine compliance of 2.1 nm/mN.

deep indentations, which were in contact with soft, strain-hardenable material. In this case, it was necessary to determine a function $\alpha = \alpha(h)$. This was done by fitting a quadratic polynomial to the observed α versus h data and extrapolating the curve to shallower depths. The uncertainty of the pile-up (or sink-in) behavior of the material at shallow depths makes the annealed sample a less suitable choice for tip calibration experiments and probably explains the slightly better agreement of the calibrations at large depths than at shallow depths.

Although a tip calibration can be obtained in the manner described above, it is still insufficient to make accurate measurements of materials that show significant strain-hardening effects. For materials that exhibit extensive pile-up or sink-in, α must be determined as a material constant or as a function of contact depth. If the modulus of the material is not known, it may be necessary to image indentations to precisely characterize its pile-up (or sink-in) behavior. If the elastic constants E and ν are well known for a material, however, and the indenter tip shape is well known, it may be possible to calculate the parameter α from the measured modulus, without having to image the indentations.

It is important to note that a large error would result if the indentations were analyzed without accounting for the difference between the actual contact area and the cross-sectional area of the indenter. The measured indentation modulus and hardness would be too high in the case of pile-up and too low in the case of sink-in. If the α for a particular sample is known, the correct reduced modulus can be calculated from Eq. (7), and the hardness will be given simply by $P_{\max}/\alpha A_i$. A plot of the hardnesses of the samples calculated with and without

TABLE I. Experimental and theoretical indentation moduli.

Material	Without correction parameter, α (GPa)	With correction parameter, α (GPa)	Vlassak and Nix[10] (GPa)
Strain-hardened Cu	155	139	129–141[a]
Annealed Cu (111)	138	140	141

Values are theoretical predictions for the (100) and (111) surfaces, respectively.

the correction parameter α is shown in Fig. 7, and the moduli of the samples calculated with and without α are compared in Table I.

IV. SUMMARY

Nanoindentation studies of strain-hardened and annealed samples of copper have revealed significant pile-up and sink-in effects, thereby causing the projected contact area between the indenter and the sample to be greater than or less than, respectively, the cross-sectional area of the indenter. To account for these effects, a new indenter tip shape calibration technique has been developed, based on both measurements of contact compliance and direct SEM measurements of the areas of large indentations. The indenter cross-sectional areas at large depths were determined from the area of the triangle defined by the indentation corners. The ratio of the contact area to the indenter area characterizes the extent of pile-up and sink-in for the material and can be used to evaluate the indenter area for depths at which the indentations cannot easily be imaged. Thus, this calibration procedure makes a clear distinction between indentation contact area and indenter cross-sectional area. Furthermore, by determining the area correction parameter α for a material from direct observation of indentations and knowing the tip shape function of the diamond indenter tip, it is possible to make absolute determinations of indentation modulus and hardness.

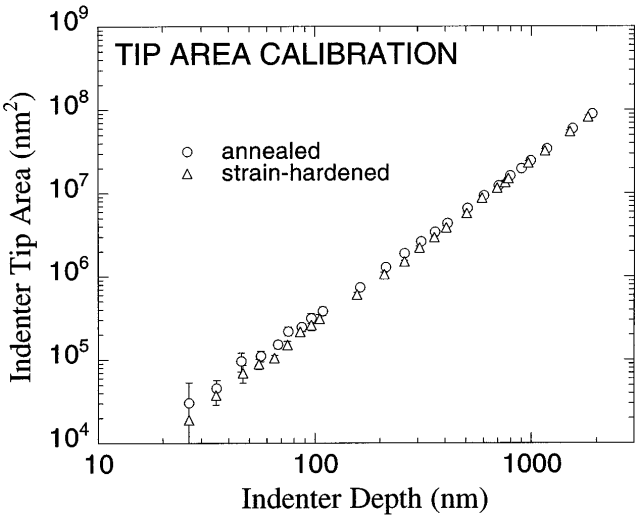

FIG. 5. A logarithmic plot of indenter tip geometry calibration as determined from experiments in the strain-hardened and annealed copper samples. The error bars represent two standard deviations.

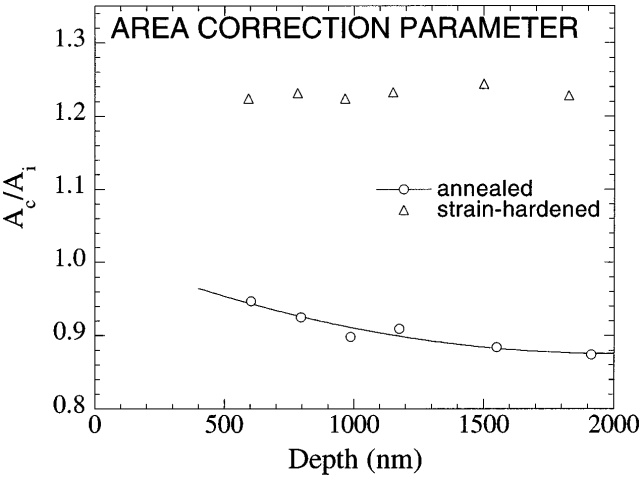

FIG. 6. The correction parameter, α, as a function of contact depth for the strain-hardened and annealed copper samples.

ACKNOWLEDGMENTS

Support for this research was provided by the Division of Materials Sciences of the Office of Basic Energy Sciences of the Department of Energy under Grant DE-FG03-89ER45387-A008 and is gratefully acknowledged.

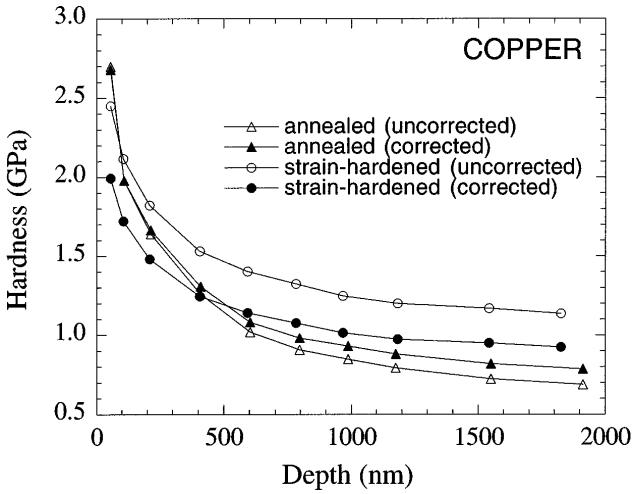

FIG. 7. Hardness versus depth as calculated from indenter cross-sectional area and contact area for strain-hardened and annealed copper.

REFERENCES

1. J. B. Pethica, R. Hutchings, and W. C. Oliver, Philos. Mag. A **48**, 593 (1983).
2. S. I. Bulychev, V. P. Alekhin, M. K. Shorshorov, A. P. Ternovskii, and G. D. Shnyrev, Zavodskaya Laboratoriya **41**, 1137 (1975).
3. S. I. Bulychev and V. P. Alekhin, Zavodskaya Laboratoriya **53**, 76 (1987).
4. M. F. Doerner and W. D. Nix, J. Mater. Res. **1**, 601 (1986).
5. M. F. Doerner, D. S. Gardner, and W. D. Nix, J. Mater. Res. **1**, 845 (1986).
6. M. F. Doerner, *Mechanical properties of metallic thin films on substrates using sub-micron indentation methods and thin film stress measurements techniques*, Ph.D. Thesis, Stanford University (1987).
7. W. C. Oliver and G. M Pharr, J. Mater. Res. **7**, 1564 (1992).
8. G. M. Pharr, W. C. Oliver, and F. R. Brotzen, J. Mater. Res. **7**, 613 (1992).
9. G. M. Pharr and W. C. Oliver, MRS Bull. **17**, 28 (1992).
10. J. J. Vlassak and W. D. Nix, J. Mech. Phys. Solids **42**, 1223 (1994).
11. M. J. Mayo, R. W. Siegel, Y. X. Liao, and W. D. Nix, J. Mater. Res. **7**, 973 (1992).
12. J. J. Vlassak and W. D. Nix, Philos. Mag. A **67**, 1045 (1993).
13. S. P. Baker and W. D. Nix, J. Mater. Res. **9**, 3131 (1994).